Available online at www.sciencedirect.com
ScienceDirect
Ceramics International 37 (2011) 3123–3131
CERAMICS INTERNATIONAL
www.elsevier.com/locate/ceramint

Mechanical properties of highly textured porous Ni–YSZ and Co–YSZ cermets produced from directionally solidified eutectics

J.J. Roa [a,b,*], M.A. Laguna-Bercero [c], A. Larrea [c], V.M. Orera [c], M. Segarra [b]

[a] Institut P' (UPR 3346), Département Physique et mécanique des matériaux, CNRS-Université de Poitiers-ENSMA, Boulevard Marie et Pierre Curie SP2MI-Téléport 2-BP 30179, F-86962 Futuroscope Chasseneuil Cedex, France

[b] Centro DIOPMA, Universidad de Barcelona, Facultad de Quimica, Departamento de Ciencia de los Materiales e Ing, Metalurgica, Marti i Franques, 1, E-08028 Barcelona, Spain

[c] Instituto de Ciencia de Materiales de Aragon, ICMA, CSIC-Universidad de Zaragoza, Pedro Cerbuna 12, E-50009 Zaragoza, Spain

Received 8 April 2011; received in revised form 14 May 2011; accepted 14 May 2011
Available online 23 May 2011

Abstract

It is well known that several ceramic materials develop an usual; and sometimes unique; combination of properties as a result of mixing different phases with similar expansion coefficients. Sometimes they are elastically stiff, have low thermal expansion coefficients, and are resistant to chemical attack. As this paper will show, their mechanical properties are also enhanced.

Nanoindentation is used to measure the mechanical properties for each phase of NiO–YSZ and CoO–YSZ eutectics produced by the laser floating zone technique, and also the analogues Ni–YSZ and Co–YSZ cermets produced by reduction from the eutectic precursors. The different tests have been performed at 100 nm, in order to obtain an imprint lower than the size of the secondary phase and extract the hardness and Young's modulus. Moreover, several tests have been performed at 2000 nm of indentation range to obtain the response of each material. The different imprints have been visualized by Atomic Force Microscopy.

Keywords: Solid Oxide Fuel Cell; Directionally solidified eutectic; Laser floating zone technique; Ceramic materials; Nanoindentation

1. Introduction

Eutectic ceramic composites produced by directional solidification from melt (DSEC) are fully dense materials with a fine and homogeneous microstructure of separated phases, lamellae, fibres or more complex morphologies, well aligned along the solidification direction. They show unusual and very different properties from those expected from simple addition of the component phases [1]. The domains in directionally solidified eutectics are single crystalline with sizes ranging from hundreds of micrometers to tens of nanometers [2] connected by clean and strong interfaces at atomic scale. Moreover, the size, λ, of the eutectic structure can often be modified by simply changing the growth rate, V, according to the law $\lambda^2 V = \text{constant}$. Ceramic eutectics have been studied because of their unpaired mechanical properties consequence of the small phase size and the high quality of interfaces. Moreover, the extraordinary regularity of the eutectic microstructure and the neatness of the interfaces usually increases the thermal stability to these compounds [3]. DSEC presents higher mechanical properties, thermal shock resistance and fracture strength than single crystals and glasses, and a better thermal stability and retention of mechanical resistance up to temperatures near to the melting point than conventional ceramic [4].

A Solid Oxide Fuel Cell (SOFC) is a device widely employed to convert the chemical energy of different types of fuel to electricity. For the anode in these devices, porous cermets of metallic nickel and yttria-stabilized cubic phase of the zirconia (YSZ) are commonly used [5,6]. The properties of these anodes are mostly dependent on their microstructure being the main concern the relatively poor mechanical properties and the tendency to coarsening of Ni particles under operation conditions. It was recently reported that highly

* Corresponding author at: Institut P' (UPR 3346), Département Physique et mécanique des matériaux, CNRS-Université de Poitiers-ENSMA, Boulevard Marie et Pierre Curie SP2MI-Téléport 2-BP 30179, F-86962 Futuroscope Chasseneuil Cedex, France.
E-mail address: jjrr_cons@hotmail.com (J.J. Roa).

0272-8842/$36.00
doi:10.1016/j.ceramint.2011.05.051

structured porous Ni–YSZ [7] and Co–YSZ [8] produced from directionally solidified NiO–YSZ and CoO–YSZ eutectics, and their subsequent reduction seem to present numerous advantages compared with conventional Ni–YSZ cermets. The stable interfaces formed between the phases during NiO–YSZ or CoO–YSZ eutectic growth and subsequent treatment of the DSE in a reducing atmosphere produces the Ni (or Co)–ZrO_2 cermet, where the Ni phase and the ZrO_2 phase are bonded by low-energy interfaces, assuring long term stability. Moreover, the channeled microstructure of this textured cermet improves the performance of the material, allowing good gas flow and electronic conduction through the Ni porous lamellae, and also provides an appropriate thermal expansion coefficient (TEC = 10.8×10^{-6} K^{-1}), thus achieving a good thermochemical integration with the YSZ electrolyte [9,10].

Thermal and mechanical strength are essential properties for these devices, as they are formed by various layers of different materials that must present high-quality integration. Experimental data on the mechanical properties of DSEC are very limited because of the small size of samples available and high stiffness of the compounds involved, which implies the need of non-standard techniques to determine the strain [1]. Moreover, the component phases are not exactly ''pure'' single crystal phases. For example, 2 mol% Ni^{2+} and 5 mol% Co^{2+} ions dissolved in the YSZ matrix during the eutectic solidification process [9]. As a consequence, determination of the mechanical properties of components is also of great interest.

Elastic properties of YSZ electrolytes and YSZ–NiO anode precursors were studied by Selçuk and Atkinson who obtained effective Young's (E_{eff}) and shear (G^*) moduli using the impulse excitation technique [11]. The mechanical properties (hardness, Young's modulus and fracture toughness) of YSZ electrolytes have been previously examined by Nanoindentation technique yielding values of 19.7–14.2 GPa, 260–223 GPa, and 1.79 MPa $m^{1/2}$, respectively [12]. Here we have studied the mechanical properties of each component phase at nanometric scale for NiO–YSZ, Ni–YSZ, CoO–YSZ, and Co–YSZ composites. In particular, those of NiO–YSZ and CoO–YSZ eutectics produced by the laser floating zone (LFZ) technique, and also the analogues Ni–YSZ and Co–YSZ cermets, produced by reduction from the eutectic precursors.

Nanoindentation is a powerful tool which allows studying the materials response at nanometric scale, by obtaining the hardness (H) and the Young's modulus (E) using the Oliver and Pharr approach. The different tests have been performed at constant penetration depths of 100 nm and 2000 nm, in order to either isolate the phase under study or to obtain the response of the composite, respectively.

In brittle materials indented with a Berkovich tip, surface examination of residual imprints by Atomic Force Microscopy (AFM) can reveal some typical features, such as: surface deformation effects (*sink-in* [13,14]), microcracks or damage inside the imprints [15], fracture mechanisms such as radial cracks emanating from the imprint corners [15], or *chipping* [16]. These effects may contribute to errors in the recorded depths and, consequently, to the hardness and modulus determination. We performed AFM studies of the imprints in order to ascertain that important aspect.

2. Experimental details

2.1. Samples preparation

Precursor ceramic cylinders, 2 mm in diameter and 10 cm in length, were prepared from a mixture of the oxides NiO (99.99%, Alfa Aesar) and 8YSZ (8 mol% Y_2O_3-stabilized ZrO_2, 99.9%, Tosoh) by cold isostatic pressing followed by sintering at 1350 °C during 12 h. Directionally solidified NiO–YSZ and CoO–YSZ eutectic rods were produced from these cylinders by the laser floating-zone method (LFZ) at a growth rate (R) of 100 mm/h. CoO–YSZ eutectics were grown under argon atmosphere in order to avoid CoO oxidation to Co_3O_4. Channeled cermets were obtained after reduction in a 5% H_2–Ar atmosphere at 850 °C. Additional details about the sample preparation method, and microstructure of the cermets, as well as on the reduction kinetics process, can be found in Laguna-Bercero et al. [7–9]. The composition of the studied materials is given in Table 1.

2.2. Microstructural characterization

The microstructure of the samples was studied using Optical Microscopy (OM). We have also performed transmission electron microscopy (TEM Model 2000FXII, Jeol, Japan) experiments on NiO (or CoO)–YSZ and Ni (or Co)–YSZ transverse-cross sections. Ion milling (Model 600dif, Gatan, Warrendale, PA) was carried out at liquid nitrogen temperatures to prevent reduction of the YSZ phase by radiation damage.

2.3. Measurement of mechanical properties with a Berkovich tipped nanoindenter

Nanoindentation tests were carried out with a Nano Indenter® XP System (Agilent Technologies) with continuous stiffness measurement, CSM (harmonic displacement 2 nm and frequency of 45 Hz). The strain rate was held constant at 0.05 s^{-1}. The different experiments were performed at room temperature using a Berkovich diamond tip and performed at a maximum applied load of 100 and 2000 nm. The indenter shape has been carefully calibrated for true penetration depths by indenting fused silica samples of known Young's modulus (72 GPa). Surface topography around nanoindentation imprints has been observed by AFM; using a Dimension 3100 microscope from Veeco (Santa Barbara, CA) in tapping mode.

Table 1
Composition calculated by image analysis (vol%) for the NiO–YSZ and CoO–YSZ eutectics, and also for the Ni–YSZ and Co–YSZ cermets.

NiO (or Ni)	YSZ	Pores	CoO (or Co)	% YSZ	Pores
	NiO–YSZ			CoO–YSZ	
56.5 ± 1.7	43.5 ± 1.7	–	61.0 ± 1.5	39.0 ± 1.5	–
	Ni–YSZ			Co–YSZ	
33.1 ± 0.7	43.5 ± 1.7	23.4 ± 0.7	34.8 ± 0.9	39.0 ± 1.5	26.2 ± 0.6

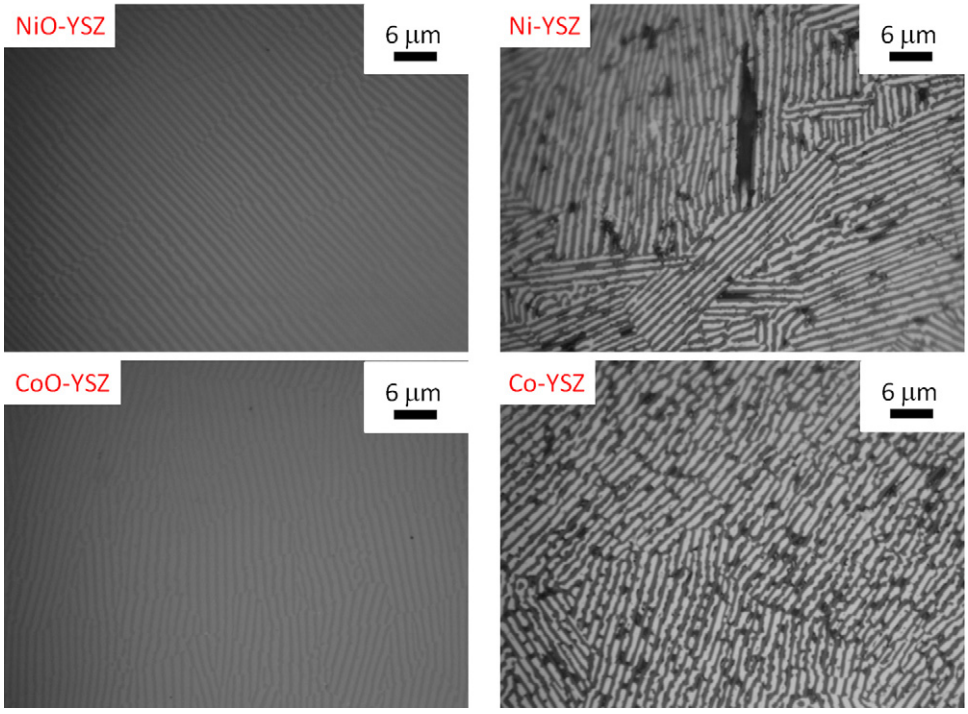

Fig. 1. Optical image of the transverse cross-section of a NiO–YSZ, CoO–YSZ DSE eutectics and also for the Ni–YSZ and Co–YSZ cermets. Bright phase: Ni (or Co); light gray phase: NiO (or CoO); dark gray phase: YSZ; dark phase: pore.

Images have been then processed with the WSxM image analysis software [17].

3. Results and discussion

3.1. Microstructure of the NiO (or CoO)–YSZ eutectics and Ni (or Co)–YSZ cermets

NiO–YSZ and CoO–YSZ eutectic rods present regular lamellar microstructure, as observed in Fig. 1. Samples are formed by eutectic grains of about 10–80 μm. Each eutectic grain consist of NiO (or CoO) lamellae (∼500 nm wide) alternating with YSZ lamellae (∼400 nm wide). The major growth crystallographic directions were [1 0 0] for YSZ and ≈[1 1 0] for NiO although growth of YSZ lamellae along the [1 1 0] directions has been also reported. At this relatively high growth rate, the YSZ–CoO eutectic grows with $[1\ 1\ 1]_{CoO}$// $[1\ 1\ 1]_{YSZ}$ [9]. The low-energy interface planes have been clearly established in the YSZ–NiO eutectic as $(1\ 1\ 1)_{NiO}$// $(0\ 0\ 2)_{YSZ}$ [9]. The interlamellar spacing ($\lambda \sim 900$ nm) is consistent with the empirical relationship $\lambda^2 R = 10^{-4}$ mm^3/h, given by Dhalenne and Revcolevschi [18]. Subsequent treatment of the NiO–YSZ and CoO–YSZ eutectics under 5%H_2/Ar atmosphere at 800 °C during 6 h produce de resulting Ni–YSZ and Co–YSZ. Under those conditions, NiO (or CoO) is reduced to metallic Ni (or Co) forming additional porosity of

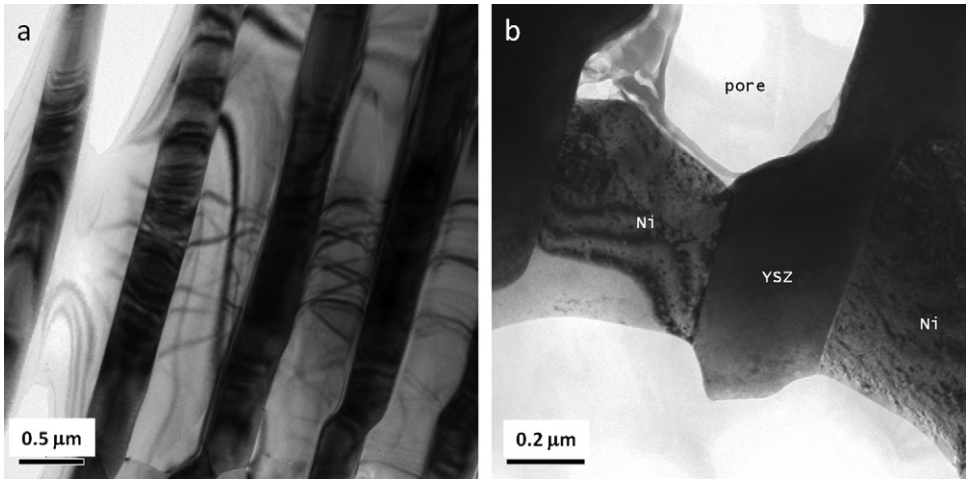

Fig. 2. TEM images for a NiO/YSZ (a) and Ni/YSZ (b) samples.

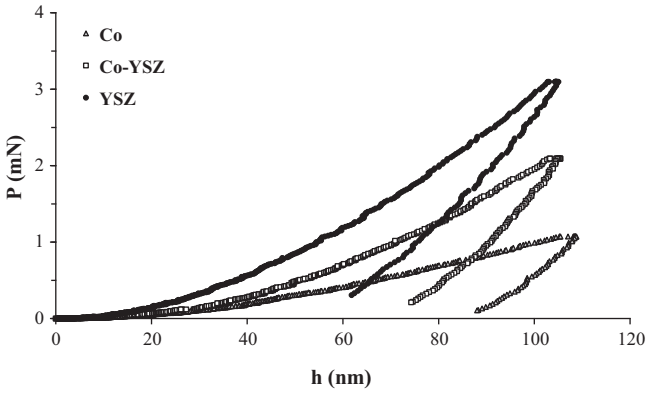

Fig. 3. Loading/unloading evolution for Co–YSZ at 100 nm of penetration depth.

23.4 vol% and 26.2 vol%, respectively. It is interesting to point out here that reduction of NiO to Ni sometimes implies a reorientation of Ni crystallographic planes [7]. Transverse cross-sections for the Ni–YSZ and Co–YSZ cermets are also shown in Fig. 1, where we can observe a homogeneous distribution on metal particles and pores constrained by the YSZ lamellae. This microstructure is more detailed in the TEM images shown in Fig. 2. Residual stresses are clearly observed for the NiO–YSZ eutectic in both NiO and YSZ phases (Fig. 2a), which are of about 1 GPa [19]. Those residual stresses, formed after solidification due to the differences on the TEC for both components, are a clear indication of the good adhesion between phases, as the stresses have not been relaxed. As pointed before, after NiO reduction the microstructure changes to form highly porous Ni lamellae. The microstructure is now highly defective and also most of the residual stresses have been relaxed, as observed in Fig. 2b. Similar results were observed for the analogues CoO–YSZ and Co–YSZ samples.

3.2. Mechanical properties

3.2.1. Loading/unloading curve

Loading/unloading curves have been measured in all the samples. Fig. 3 displays typical loading/unloading curve for Co–YSZ. This plot supplies qualitative information about the *H* and *E* for each phase. As it can be seen, the YSZ phase presents a larger applied load than the other two different phases, then this phase will be the hardest one. However, the porous metallic phase, *Co* in this case, will be the softest phase. In other words, the YSZ and the metal will present different deformation mechanisms; one brittle and the other one ductile, respectively. Each phase presents different deformation mechanisms under a compression tests. However, the Co–YSZ phase presents an interaction of each phase, so the mechanical properties present a contribution of each phase. Therefore, the Young's modulus is correlated with the slope during the unloading curve. In these cases we cannot get any qualitative conclusion.

3.2.2. Hardness and Young's modulus

Figs. 4 and 5 exhibit the *H* and the *E* evolution, respectively from 0 to 100 nm of penetration depth for each material of study and each phase. As expected, the hardness is smaller in the metallic phase. Figs. 6 and 7 show the *H* and *E* evolution for the composite at 2000 nm of indentation depth. As it is shown in Figs. 5 and 7, the Young's modulus increases when the indentation depth increases until a value, which remains

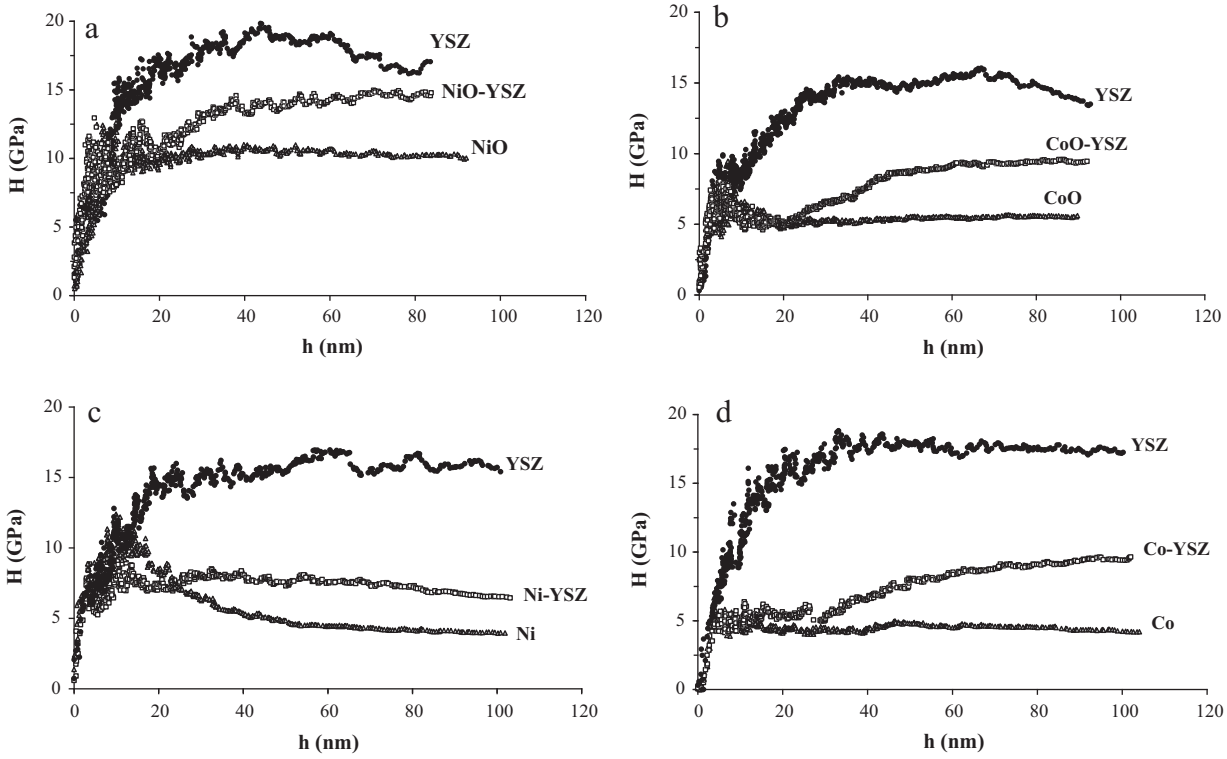

Fig. 4. Hardness evolution for each phase present in: (a) NiO–YSZ, (b) CoO–YSZ, (c) Ni–YSZ, and (d) Co–YSZ at 100 nm of indentation depth.

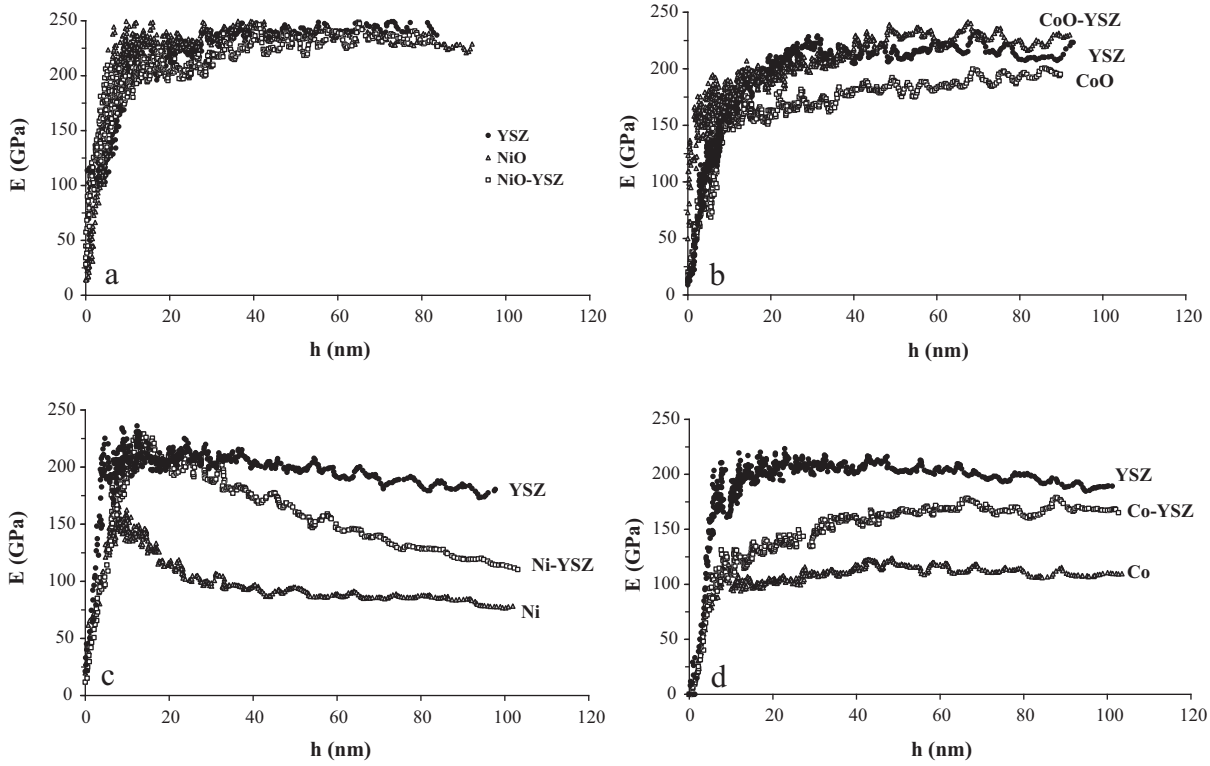

Fig. 5. Young's modulus evolution for each phase present in: (a) NiO–YSZ, (b) CoO–YSZ, (c) Ni–YSZ, and (d) Co–YSZ at 100 nm of indentation depth.

constant with indentation depth. Saturation values correspond to the true Young's modulus. For the low indentation depth case (100 nm), the Young's modulus remains constant after 50 nm depth. However, for the higher indentation depth case (2000 nm), Young's modulus increases with depth until 250 nm for NiO–YSZ and CoO–YSZ.

The behaviour is completely different in the case of metallic cermets. For the Ni–YSZ and Co–YSZ samples, the Young's modulus increases, reaches a maximum and then decreases with indentation depth. These phenomena could be attributed to a relatively poor adherence between the porous metallic lamellae and the ceramic scaffold, and also to the highly defective microstructure (Fig. 2b). This relatively bad interface will act as a microcrack between both phases and an elastic dissipation of the elastic energy could be produced yielding this instability inside of each material.

Table 2 shows the values of H and E for each phase present in the samples studied at 100 and 2000 nm of maximum penetration depth.

In the case of YSZ, the data obtained by nanoindentation for H are higher than those reported by Dahl et al. [20] (12.4–13.5 GPa), using a Vickers microindenter, and also comparable with the values around 16 GPa reported by Menvie Bekale et al. [21] using microindentation. In any case, measured hardness for YSZ lamellae are in agreement with reported values of 13–20 GPa [22–25] for YSZ bulk samples. However, the H values reported for NiO–YSZ by Roa et al. [25] for bulk NiO–YSZ ceramics (6.9–7.5 GPa) are lower than the values obtained for NiO lamellae in this manuscript (13.8 GPa). This difference could be attributed to the higher density of the eutectics (100% dense) and also to the lamellar orientation of the component phases. As can be observed in Fig. 3a, until 40 nm of

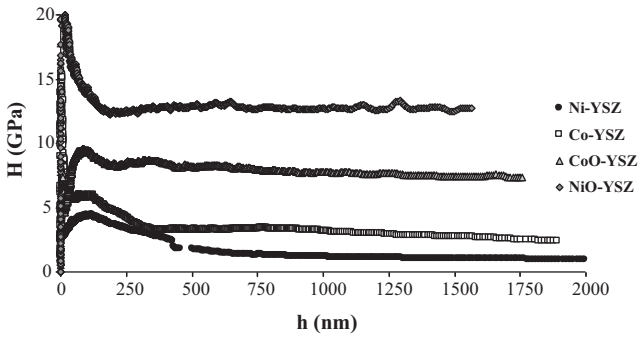

Fig. 6. Hardness evolution for each sample performed at 2000 nm of indentation depth.

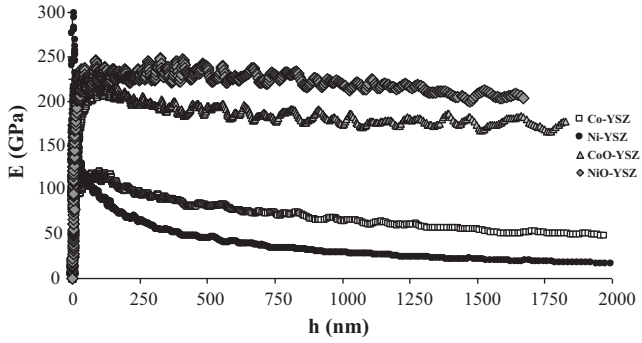

Fig. 7. Young's modulus evolution for each sample performed at 2000 nm of indentation depth.

Table 2
H and *E* values for NiO–YSZ, CoO–YSZ, Ni–YSZ and Co–YSZ for indentation depths of 100 and 2000 nm.

Sample	Phase	h = 100 nm		h = 2000 nm	
		H (GPa)	E (GPa)	H (GPa)	E (GPa)
Co–YSZ	Co	3.9 ± 0.2	102 ± 2	–	–
	YSZ	16.9 ± 0.8	179 ± 5	–	–
	Co–YSZ	9.4 ± 0.4	159 ± 3	5.9 ± 0.6	60 ± 2
Ni–YSZ	Ni	3.7 ± 0.3	65 ± 4	–	–
	YSZ	15.4 ± 0.2	180 ± 5	–	–
	Ni–YSZ	6.9 ± 0.4	110 ± 3	1.0 ± 0.1	20 ± 1
CoO–YSZ	CoO	5.4 ± 0.2	100 ± 2	–	–
	YSZ	12.5 ± 0.2	190 ± 5	–	–
	CoO–YSZ	8.8 ± 0.2	165 ± 4	8.5 ± 0.5	185 ± 7
NiO–YSZ	NiO	9.5 ± 0.4	215 ± 3	–	–
	YSZ	17.5 ± 0.4	220 ± 5	–	–
	NiO–YSZ	13.8 ± 0.2	219 ± 4	12.6 ± 0.3	215 ± 4

indentation depth exists a strong interaction between the different lamellae.

Young moduli are compared with data for the individual phases taken from literature and those calculated for the composite using the limits for isostrain (maximum) and isostress (minimum) approaches (Table 3):

$$E = E_a V_a + E_b V_b \tag{1}$$

$$\frac{1}{E} = \frac{V_a}{E_a} + \frac{V_b}{E_b} \tag{2}$$

where E_i and V_i are the Young modulus and volume fractions of phase a and b, respectively.

The Young's modulus for NiO measured by nanoindentation is close to 220 GPa given by Radovic and Lara-Curzio [27] and Giraud and Canel [26]. The *E*-values for the eutectic NiO–YSZ also agree well with the value calculated for the composite. However the value obtained for CoO is smaller than that given in the literature. The Young's modulus obtained using this technique depends of the Poisson's ratio, the porosity surrounding the region of study and under the imprint and the correct calibration of the contact area of the Berkovich tip using a standard of fused silica.

In the reduced samples nanoindentation gives slightly smaller *E*-values for the YSZ phase than in the eutectic. The decrease in the Young modulus of the metallic phases could be due to the porosity. Effect of porosity in the effective moduli of SOFC materials has been study by Selçuk and Atkinson [11]. There are some empirical relations expressing the Young modulus as a function of porosity. The linear relationship is widely used for low porosity levels:

$$E = E_0(1 - b_E p) \tag{3}$$

here E_0 is the bulk Young modulus for the dense materials, p is the volume porosity and b_E a fitting parameter defining the porosity dependence of the modulus. Measurements of E as a function of porosity have been done in both NiO–YSZ ceramics and Ni–YSZ cermets being b_E 2.12 and 1.75, respectively [27]. Assuming the last value to be valid for both Ni–YSZ and Co–YSZ cermets, we estimated the Young modulus of cermets in Table 3.

Table 3
Bulk *E*-values for the component phases taken from literature and theoretical *E*-values of the eutectics and porous cermets (see text).

	YSZ [11]	NiO	Ni	CoO	Co
E (GPa)	220	220	220	170	209
	NiO–YSZ	CoO–YSZ	Ni–YSZ		Co–YSZ
E (GPa)	220	186.5–189.5	129.3		101.8

The Young's modulus for the cermet Ni–YSZ, 110 GPa, is slightly smaller than that calculated for the theoretical porosity given in Table 3, but higher than the values reported by Giraud et al. [26] at room temperature, 85 GPa. However, Radovic and Lara-Curzio [27] report a value as small as 55 GPa for a cermet with 40% of porosity and containing 63 wt% of NiO before the reduction process.

As it can be seen in Table 2, the different values obtained at maximum indentation depth are in agreement with the previous values obtained at 100 nm depth in the case of unreduced samples, NiO–YSZ and CoO–YSZ. These materials do not present size effect [28] because they are dense materials without internal stresses and with a good adherence between phases as corresponds to DSEC ceramics. The Young's modulus remains stable at very low indentation depths.

However, for the reduced samples the mechanical properties present an strong size effect dependence. This effect could be attributed to the presence of interface defects generated during the reduction process due to: (i) different expansion coefficients between the metallic and ceramic lamella yielding a high amount of dislocations at the vicinity of the interface, (ii) high amount of stresses generated in the interphase interface, and (iii) internal porosity which modifies the plastic and the elastic mechanical response.

As a summary, the E as well as H of these materials, measured by nanoindentation, were higher than those reported by conventional techniques (Vickers indentation, bending, etc.). Another possibility is that by this technique we measure local mechanical properties due to the small volume of study, and at this scale we only study pure phases without the influence of macroscopic defects or secondary phases.

3.3. Imprints visualization

Fig. 8 shows AFM images of a CoO–YSZ eutectic sample surface, perpendicular cut to the growth direction, in which indentation imprints have been performed at 100 nm of indentation depth. AFM reveals the presence of YSZ and CoO-lamella of about 500 nm width homogeneously distributed in the textured sample. However, they cannot be easily associated to a particular eutectic component using a conventional tool like macro/microindentation technique due to the fact that the residual size of the imprint will be larger than the size of each individual phase. On the contrary, the present technique allows performing indentation imprints with depths

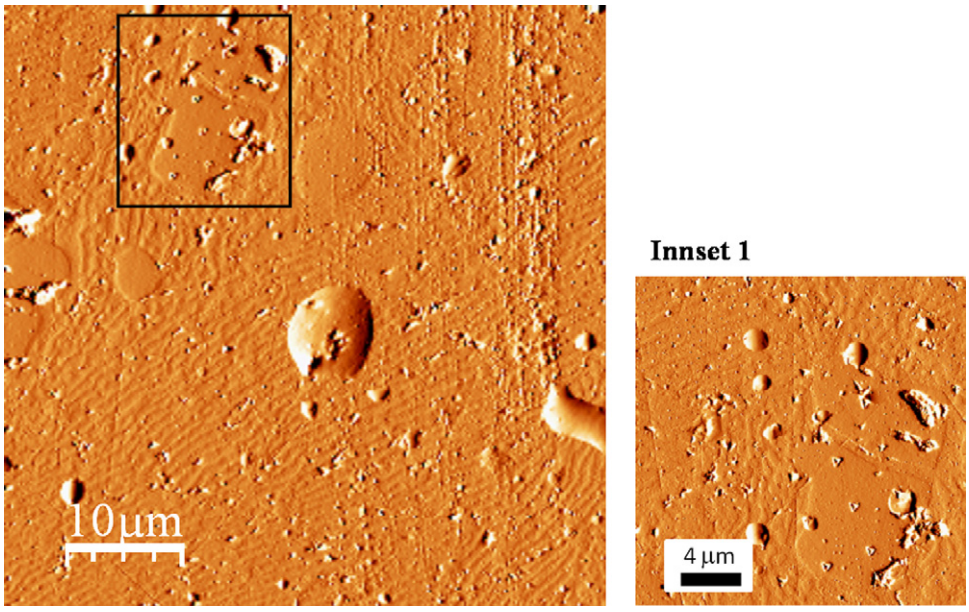

Fig. 8. AFM-error micrographs of residual imprints performed at 100 nm of indentation depth in the CoO–YSZ. Inset 1: magnification of a YSZ grain with several imprints.

of several nanometers, which allows us to isolate the mechanical behaviour of each phase. Inset 1 in Fig. 8, shows a magnification of the region marked with a black square where several imprints have been performed inside a YSZ grain. This is a particular experiment that allows us to unequivocally identify the properties of the YSZ phase in the case of individual YSZ lamellae.

After the mechanical characterization, the AFM observation of the different imprints permits to study the different fracture mechanisms taking place during the indentation process. As an example, Fig. 9 shows different residual imprints in a YSZ-grain in Co–YSZ samples performed at 100 nm of indentation depth. As it can be seen, all imprints present a field strain in the vicinity of the residual imprint. A magnification of one imprint can be observed in the inset 1. This deformation mechanism activated during the indentation process is called chipping. In addition, this figure illustrates the presence of several cracks at the corners of the imprint due to the field stress generated during the indentation process.

Fig. 10 exhibits a residual imprint performed at 2000 nm of indentation depth in Co–YSZ (Fig. 10a) and CoO–YSZ (Fig. 10b) samples. As it can be seen, in both cases the size of the residual imprint overcomes that of lamella. At that indentation depth it is impossible to isolate the contribution of each phase, and only a macroscopic behaviour of each material can be obtained. Fig. 10a shows an abnormal

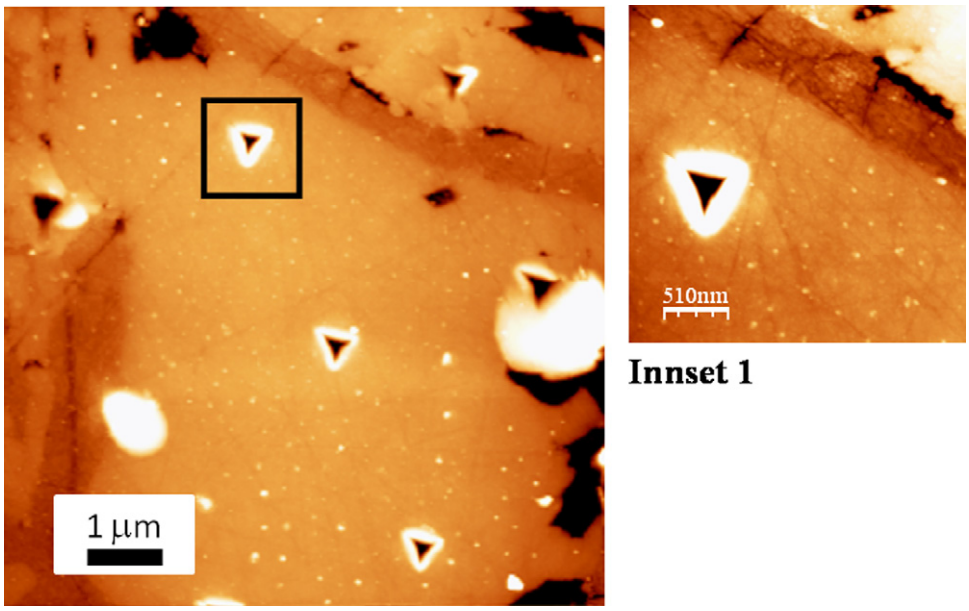

Fig. 9. Topographic image for an YSZ-grain performed in Co–YSZ samples. Inset 1: magnification of one of the residual imprints.

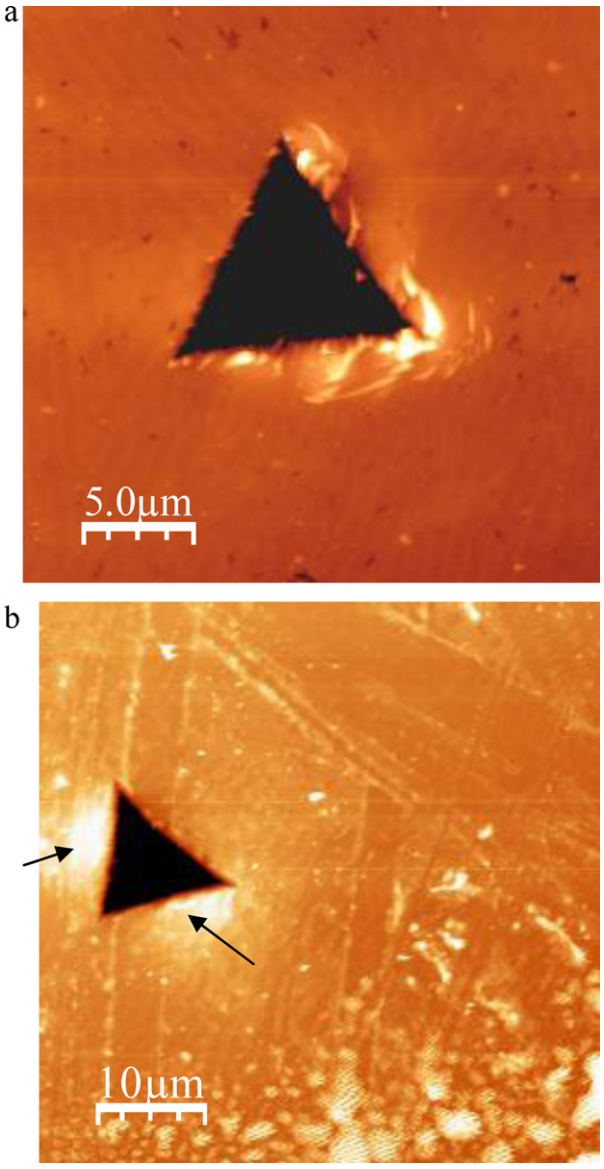

Fig. 10. AFM-topography image of residual imprint performed at 2000 nm of indentation depth for (a) Co–YSZ and (b) CoO–YSZ.

behaviour (like a kink) at the boundary of the imprint. This effect could be attributed to the ductile behaviour introduced by the metallic phase (Co). Consequently, this behaviour was not observed in CoO–YSZ sample (see Fig. 10b). In this case the plastic field can be clearly observed at two sides of the imprints denoted with black arrows.

4. Conclusions

Nanoindentation at maximum indentation depth of 100 nm, and using the Oliver and Pharr approach, allows us to determine the hardness and Young's modulus for each phase present in some well-known SOFC materials: NiO–YSZ, CoO–YSZ, Ni–YSZ and Co–YSZ. Directionally solidified eutectics have been obtained for each phase separately. The YSZ phase is harder than the oxide (NiO and CoO) and metallic (Ni and Co) phases.

The Young's modulus and hardness values for the interphase are in correct agreement with different values reported in the literature obtained using sharp indentations.

Nanoindentation at low indentation depth (around 100 nm) allows us to isolate the; mechanical properties for each phase yielding the following hardness and Young's modulus values for each phase, respectively: NiO–YSZ (NiO = 9.5 and 215 GPa, YSZ = 17.5 and 220 GPa), Ni–YSZ (Ni = 3.7 and 65 GPa, YSZ = 15.4 and 180 GPa), CoO–YSZ (CoO = 5.4 and 100 GPa, YSZ = 12.5 and 190 GPa) and (Co = 3.9 and 102 GPa, YSZ = 16.9 and 179 GPa). This indentation depth allows to isolate the mechanical properties due to the size of the residual imprint is smaller than the length of each phase.

However, the measurements performed at 2000 nm do not permit to difference each phase, due to the size of the residual imprint which is higher than the thickness of each phase.

Acknowledgements

We would like to thank Spanish Government and the FEDER program within the projects: MAT2008-06785-C02-01, MAT2009-14324-C02-01, GA-LC-009/2009, CEN20071018 and CIT-120000-2007-50, by the financial support and Serveis Cientificotècnics (Universidad de Barcelona) for AFM data. J.J. Roa would like to thank Dr. Emilio Jiménez-Piqué (Centre d'Integritat Estructural i Fiabilitat dels Materials, UPC) for experimental data.

References

[1] J. Llorca, V.M. Orera, Directionally solidified eutectic ceramic oxides, Prog. Mater. Sci. 51 (2006) 711–809.
[2] P.B. Oliete, J.I. Peña, A. Larrea, V.M. Orera, J. Llorca, J.Y. Pastor, A. Martín, J. Segurado, Ultra-high-strength nanofibrillar Al_2O_3–YAG–YSZ eutectics, Adv. Mater. 19 (2007) 2313–2318.
[3] A. Sayir, S.C. Farmer, P.O. Dickerson, A.M. Yun, High temperature mechanical properties of $Al_2O_3/ZrO_2(Y_2O_3)$ fibers, Mater. Res. Soc. Symp. Proc. 365 (1993) 21–27.
[4] Y. Waku, N. Nakagawa, T. Wakamoto, H. Ohtsubo, K. Shimizu, Y. Kohtoku, A ductile ceramic eutectic composite with high strength at 1873 K, Nature 389 (1997) 49–52.
[5] B.C.H. Steele, A. Heinzel, Materials for fuel-cell technologies, Nature 414 (2001) 345–352.
[6] S.C. Singhal, K. Kendall (Eds.), High Temperature Solid Oxide Fuel Cells: Fundamentals, Design, and Applications, Elsevier, 2003.
[7] M.A. Laguna-Bercero, A. Larrea, R.I. Merino, J.I. Peña, V.M. Orera, J. Am. Ceram. Soc. 88 (11) (2005) 3215–3217.
[8] M.A. Laguna-Bercero, A. Larrea, R.I. Merino, J.I. Peña, V.M. Orera, J. Eur. Ceram. Soc. 28 (2008) 2325–2329.
[9] M.A. Laguna-Bercero, A. Larrea, J.I. Peña, R.I. Merino, V.M. Orera, Structured porous Ni– and Co–YSZ solidified eutectic composites, J. Eur. Ceram. Soc. 25 (2005) 1455–1462.
[10] G. Garcia, R.I. Merino, V.M. Orera, A. Larrea, J.I. Peña, M.A. Laguna-Bercero, J.A. Pardo, J. Santiso, A. Figueras, YSZ thin films deposited on NiO-CSZ anodes by pulsed injection MOCVD for intermediate temperature SOFC applications, Chem. Vap. Depos. 10 (2004) 249–252.
[11] A. Selçuk, A. Atkinson, Elastic properties of ceramic oxides used in solid oxide fuel cells, J. Eur. Ceram. Soc. 17 (1997) 1523–1532.
[12] M. Morales, J.J. Roa, X.G. Capdevila, M. Segarra, S. Pinol, Mechanical properties at nanometer scale of GDC and YSZ used as electrolytes for solid oxide fuel cells, Acta Mater. 58 (2010) 2504–2509.

[13] K.L. Johnson, The correlation of indentation experiments, J. Mech. Phys. Sol. 18 (1970) 115–126.
[14] J. Alcalá, A.C. Barone, M. Anglada, The influence of plastic hardening on surface deformation modes around Vickers and spherical indents, Acta Mater. 48 (2000) 3451–3464.
[15] Z. Burghard, A. Zimmermann, J. Rödel, F. Aldinger, B.R. Lawn., Crack opening profiles of indentation cracks in normal and anomalous glasses, Acta Mater. 52 (2004) 293–297.
[16] B.R. Lawn, M.V. Swain, K. Phillips, On the mode of chipping fracture in brittle solids, J. Mater. Sci. Lett. 10 (1975) 1236–1239.
[17] I. Horcas, R. Fernandez, J.M. Gomez-Rodriguez, J. Colchero, J. Gomez-Herrero, A.M. Baro., WSxM: a software for scanning probe microscopy and a tool for nanotechnology, Rev. Sci. Instrum. 78 (1) (2007), 013705, 8 pp.
[18] G. Dhalenne, A. Revcolevschi, Directional solidification in the NiO–ZrO_2 system, J. Cryst. Growth 69 (1984) 616–618.
[19] E.C. Dickey, V.P. Dravid, C.R. Hubbard, Interlamellar residual stresses in single grains of NiO–ZrO_2(cubic) directionally solidified eutectics, J. Am. Ceram. Soc. 80 (11) (1997) 2773–2780.
[20] P. Dahl, I. Kaus, Z. Zhao, M. Johnson, M. Nygren, K. Wiik, T. Grade, M.-A. Einarsrud, Densification and properties of zirconia prepared by three different sintering techniques, Ceram. Int. 33 (2007) 1603–1610.
[21] V. Menvie Bekale, G. Sattonnay, C. Legros, A.M. Huntz, S. Poissonnet, L. Thomé, Mechanical properties of cubic zirconia irradiated with swift heavy ions, J. Nucl. Mater. 384 (2009) 70–76.
[22] L. Donzel, S.G. Roberts, J. Eur. Ceram. Soc. 20 (2000) 2457–2462.
[23] H. Jiang, Y. Lu, W. Huang, X. Li, M. Li., Mater. Charact. 51 (2003) 1–10.
[24] S. Tekili, Comp. Sci. Technol. 65 (2005) 967–972.
[25] J.J. Roa, J.C. Ruiz-Morales, J. Canales-Vázquez, M. Morales, X.G. Capdevila, P. Núñez, M. Segarra, Mechanical characterization at nanometric scale of a new design of SOFCs, Fuel Cells 11 (2011) 124–130.
[26] S. Giraud, J. Canel, Young's modulus of some SOFCs materials as a function of temperature, J. Eur. Ceram. Soc. 28 (2008) 77–83.
[27] M. Radovic, E. Lara-Curzio, Elastic properties of nickel-based anodes for solid oxide fuel cells as a function of the fraction of reduced NiO, J. Am. Ceram. Soc. 87 (2004) 2242–2246.
[28] J.J. Roa, A. Magraso, M. Morales, P. Núñez, M. Segarra, Determination of hardness, Young's modulus and fracture toughness of lanthanum tungstates as novel proton conductors, Ceram. Int. 37 (2011) 1593–1599.